Bulletin of the Seismological Society of America, Vol. 99, No. 6, pp. –, December 2009, doi: 10.1785/0120080038

Correlations of Seismicity Patterns in Southern California with Surface Heat Flow Data

by Bogdan Enescu,* Sebastian Hainzl, and Yehuda Ben-Zion

Abstract We investigate the relations between properties of seismicity patterns in Southern California and the surface heat flow using a relocated earthquake catalog. We first search for earthquake sequences that are well separated in time and space from other seismicity and then determine the epidemic type aftershock sequence (ETAS) model parameters for the sequences with a sufficient number of events. We focus on the productivity parameter α of the ETAS model that quantifies the relative efficiency of an earthquake with magnitude M to produce aftershocks. By stacking sequences with relatively small and relatively large α values separately, we observed clear differences between the two groups. Sequences with a smaller α have a relatively large number of foreshocks and relatively small number of aftershocks. In contrast, more typical sequences with larger α have relatively few foreshocks and larger number of aftershocks. The stacked premainshock activity for the more typical latter sequences has a clear increase in the day before the occurrence of the main event. The spatial distribution of the α values correlates well with the surface heat flow: areas of high heat flow are characterized by relatively small α, indicating that in such regions the swarm-type earthquake activity is more common. Our results are compatible with a damage rheology model that predicts swarm-type seismic activity in areas with relatively high heat flow and more typical foreshock–mainshock–aftershock sequences in regions with normal or low surface heat flow. The high variability of α in regions with either high or low heat flow values indicates that at local scales additional factors (e.g., fluid content and rock type) may influence the seismicity generation process.

Introduction

The diversity of seismicity patterns together with the difficulty of establishing if certain variations of seismic activity are genuine, are statistically significant, and correlate with some physical observables are important reasons why the processes that control the occurrence of earthquakes are poorly understood and under continuous debate.

A remarkable characteristic of earthquake activity is its clustering as a function of time and space. Mogi (1963) distinguished the following three main types of earthquake sequences based on their temporal characteristics: (1) sequences with a mainshock and both foreshocks and aftershocks, (2) sequences with a mainshock and aftershocks, and (3) earthquake swarms. He found that these sequence types were dominant in different parts of Japan and interpreted the differences in terms of regional variations of heterogeneity at the source region.

*Now at: Earthquake Research Department, National Research Institute for Earth Science and Disaster Prevention (NIED), 3-1 Tennodai, Tsukuba, Ibaraki, 305-0006, Japan

While the majority of earthquake sequences have a clear mainshock (i.e., clear largest event), some clusters of earthquakes that occur in a relatively short period of time have no obvious mainshock. Such bursts of seismicity are known as earthquake swarms (e.g., Richter, 1958; Mogi, 1963; Vidale and Shearer, 2006). They are often attributed to fluids, magma migration, or aseismic slip (e.g., Sykes, 1970; Nur, 1974; Hainzl, 2003, 2004; Hainzl and Ogata, 2005; Lohman and McGuire, 2007). However, it is not clear yet what are the key factors that control the occurrence of earthquake swarms.

One basic difference between more typical earthquake sequences and swarms is the relative ability or efficiency of an earthquake of a certain magnitude to generate subsequent offspring (or aftershocks in a general sense). The parameter α of the epidemic type aftershock sequence (ETAS) model (Ogata 1985, 1988) described further in the Analysis Method section quantifies the relative aftershock efficiency (or productivity) as a function of the mainshock magnitude. Ogata (1987) analyzed several worldwide earthquake data sets and concluded that swarm-type activity has a smaller

α value than that of ordinary mainshock and aftershock sequences. Christophersen and Smith (2008) studied the relation between foreshock rates and the abundance of aftershocks, which is a function of the α and b values of the frequency–magnitude distribution (Gutenberg and Richter, 1944). In this work, we take advantage of the recent progress in earthquake relocations based on waveform cross correlation (Lin *et al.*, 2007) to study in detail the variations of the α parameter in Southern California, using earthquake sequences that are well separated in space and time. We explore the ability of the parameter α to distinguish between typical earthquake sequences and swarms and investigate whether the spatial distribution of α correlates with observed surface heat flow data. The obtained results are compared with predictions of the viscoelastic damage rheology model of Ben-Zion and Lyakhovsky (2006) for properties of aftershock
sequences.

Data

We use the Southern California earthquake catalog of Lin *et al.* (2007), which contains 433,166 events that occurred between 1981 and 2005. The catalog was obtained using a new 3D velocity model and waveform cross correlation to improve the location of earthquakes. We removed from the original catalog 27,454 quarry blast events, marked as such in the catalog, and limit our analysis to the square area defined by 32.50°–38.09° latitude and −113.58°– −121.76° longitude. We estimate the magnitude of completeness M_c 2.0 as the magnitude for which 95% of the data can be modeled by a power-law fit, following the procedure of Wiemer and Wyss (2000). We remove from the original catalog all earthquakes with magnitudes $M < 2.0$, ending up with a data set of 92,587 events. The same magnitude of completeness has been used in other studies (e.g., Helmstetter *et al.*, 2005) for regions of similar spatial extent. The magnitude of completeness, however, may change significantly as a function of time and space (e.g., Enescu and Ito, 2002; Woessner and Wiemer, 2005; Schorlemmer and Woessner, 2008). Aftershock sequences, in particular, could be significantly incomplete at short times after a larger mainshock, as discussed in several recent studies (e.g., Kagan, 2004; Peng *et al.*, 2006; Enescu *et al.*, 2007; Peng *et al.*, 2007; Enescu *et al.*, 2009). To eliminate incomplete earthquake data from correlations with the crustal heat flow, we use only sequences with an Omori–Utsu c value (see, e.g., equation 4 subsequently) larger than a threshold, discussed in detail in the Results section. While this analysis insures that in general the obtained results are not biased by data incompleteness, we also tested our findings using higher M_c values, ranging from 2.1 to 2.4.

The heat flow data is taken from the U.S. Geological Survey (USGS) online heat flow database (see the Data and Resources section). Figure 1 shows a map view of the employed seismicity ($M \geq 2.0$) and heat flow data.

Analysis Method

We first search for earthquake sequences that are well separated from others seismicity in space and time using the procedure explained previously. Then we estimate the space-independent ETAS parameters for each separated sequence, together with their confidence intervals. We chose this combined approach instead of using a space-dependent ETAS model for the whole data set because it allows us to determine not only the spatial but also possible temporal changes of the ETAS parameters and avoids spatial smoothing. Fitting the space-dependent ETAS model to empirical data often yields α values that are significantly smaller than results based on stacking of aftershock sequences (e.g., Felzer *et al.*, 2004; Helmstetter *et al.*, 2005). Hainzl *et al.* (2008) showed with synthetic simulations that this is likely to result from assuming spatial isotropy for the aftershock distributions, which in reality tend to align along the mainshock ruptures. However, the application of the space-independent ETAS model produces unbiased estimations of the α value and other model parameters (Hainzl *et al.*, 2008).

The separation into clusters is done using a similar method to that used by Vidale and Shearer (2006) and Peng (2007) and described in detail subsequently. An event is considered a mainshock if it is not preceded or followed by larger earthquakes within a spatial window of radius R and a temporal window of T days. We consider here only sequences with mainshock magnitudes between 3.5 and 6.0, although we checked the results for lower magnitude thresholds from 3.0 to 3.5 and upper magnitude limits between 5.5 and 6.0. The use of circular regions to represent aftershock areas is considered appropriate for mainshocks with $M \leq 6.0$, which generally do not saturate the seismogenic zone.

We determine the rupture radius, r, of each earthquake using the scaling relation for a circular crack with a uniform stress drop (e.g., Ben-Zion, 2003):

$$r = (P_0/c\Delta\varepsilon_S)^{1/3}, \tag{1}$$

where P_0 is the scalar seismic potency of the event, $\Delta\varepsilon_S$ is the static strain drop assumed here to be 10^{-4}, and $c = 2.283$. The P_0 value of each event is calculated from the empirical potency-magnitude formula of Ben-Zion and Zhu (2002):

$$\log_{10} P_0 = 0.06M_L^2 + 0.98M_L - 4.87, \tag{2}$$

with M_L being the magnitude of the event, and P_0 is in km^2 cm. The radius R of the influence window of each event is taken as $f \times r$, with f being a constant. We also used a different approach, estimating the rupture length L as a function of magnitude M (Working Group on California Earthquake Probabilities, 2003; Helmstetter *et al.*, 2005),

$$L(M) = 0.01 \times 10^{0.5M} \text{ (km)}, \tag{3}$$

and then multiplying L with a constant f to estimate R.

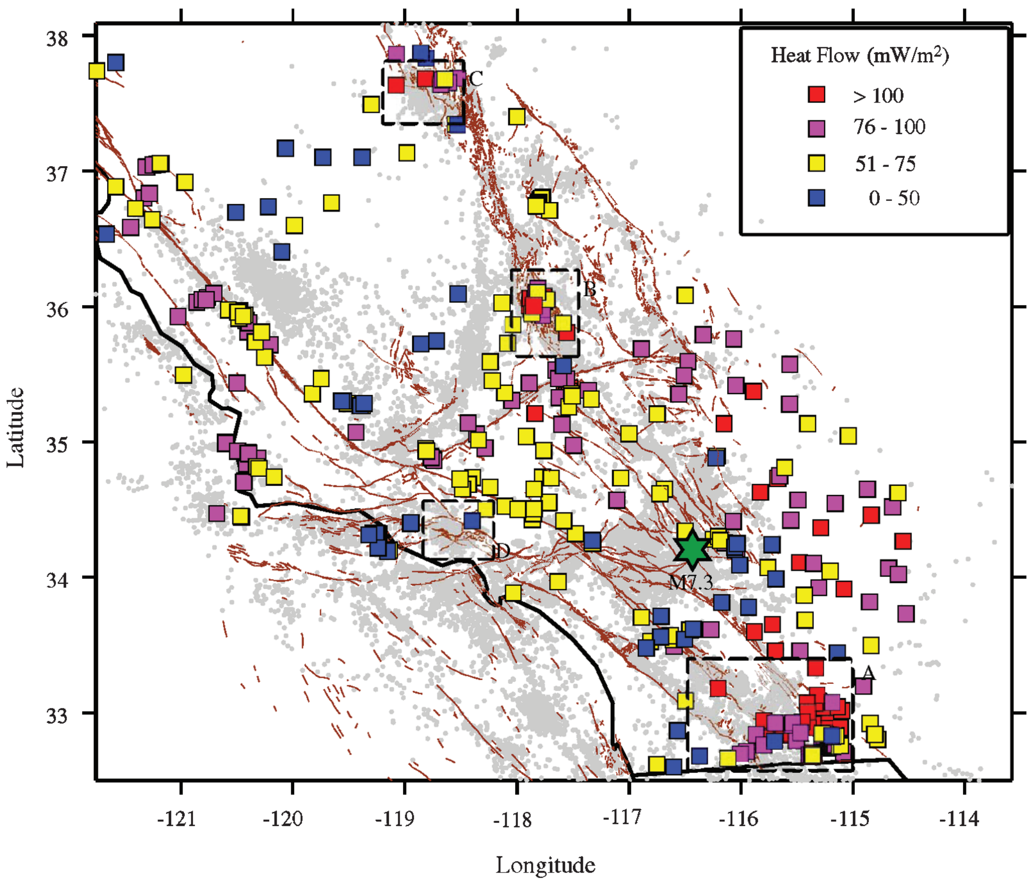

Figure 1. A map view showing epicenter locations (gray dots) for earthquakes with $M \geq 2.0$ and heat flow data (colored squares with values indicated in the legend) used in this work. The earthquakes are from the catalog of Lin *et al.* (2007) and the heat flow values are from the USGS heat flow database. The A, B, C, and D rectangles indicate areas for which the α values are discussed in the text in relation with the heat flow data.

We found that the method employed to estimate the source dimension has no significant effect on the selection of earthquake sequences, but the multiplying constant f has some effect on the number of separated clusters and the number of events in each cluster. For the results presented in this article, we chose $f = 5$ with the first approach (equations 1 and 2). Comparison between the R values with the radius of influence that is used in declustering algorithms (e.g., Reasenberg, 1985) shows that these values are comparable. The radius of the influence window takes values of 11.3 and 21.5 km for earthquake magnitudes of 5.5 and 6.0, respectively. To account for possible dynamic triggering of small events well beyond the traditional rupture length (e.g., Felzer and Brodsky, 2006), we set the minimum value of R to be 10 km (Peng, 2007).

The number of earthquakes in each sequence is obviously dependent on the length of the time window T. We tested several values for $T = 50$, 100, 150, and 200 days. For increasingly large temporal windows, the total number of separated sequences decreases and, in most cases, at times larger than about 50 days from the mainshock there is mainly background seismicity. We decided to use a time window $T = 100$ days and determine the ETAS parameters for each of the resulting sequences.

To assess whether our parameter estimations could be biased by including in the ETAS modeling time periods when the background seismicity is dominant, we also performed some additional testing. We separated earthquake clusters using the same spatial radius as before but with a shorter time window of 50 days. The shorter time window (i.e., 50 instead of 100 days) was chosen to slightly increase the number of separated sequences; however, larger windows lead to similar results. For each separated sequence, we selected only the events that occurred within 20 days from the corresponding mainshock and determined the ETAS parameters for these data.

To avoid selecting sequences that are composed mainly of aftershock activity of previous large events, we impose the additional condition that within 5 km from the mainshock and between 100 and 5 days before the occurrence of the main event there should be less than $N_{bg} = 15$ events in the sequence. We present results using also the more restrictive condition of $N_{bg} = 5$ events. Using the approach outlined previously, several hundred sequences are selected, but many of them contain only a few events. For further quantitative analysis with the ETAS model described subsequently, we use sequences that have more than 30 events. The Results section presents first detailed results obtained using sequences spanning from −100 days before to 100 days after the mainshock. Then it discusses results obtained using sequences spanning from −20 days to 20 days relative to the mainshock. For both cases, we show results obtained using $N_{bg} = 15$ and $N_{bg} = 5$.

The aftershocks rate (λ) is generally described by the Omori–Utsu law:

$$\lambda(t) = \frac{K}{(t+c)^p}, \tag{4}$$

where K, c, and p are constants, and t is the elapsed time since the mainshock (for a review, see Utsu *et al.*, 1995). Extending this model, Ogata (1985, 1988) proposed the ETAS model to describe the ongoing seismic activity in a region. In this model, the rate of seismicity at time t is given by a superposition of a constant background seismicity rate (μ) and the Omori–Utsu functions (4) of any shock i that occurred at time $t_i < t$:

$$\lambda(t) = \mu + \sum_{t_i<t} \frac{K_i}{(t - t_i + c)^p}. \tag{5}$$

The productivity parameter K_i is dependent on the magnitude M_i, as well as the cutoff magnitude M_0 of the data set according to the following function:

$$K_i = K_0 e^{\alpha(M_i - M_0)}. \tag{6}$$

One justification for relation (6) is that the aftershock area was found to grow exponentially with the magnitude of the mainshock (Utsu and Seki, 1955) and so does the number of aftershocks (Kanamori and Anderson, 1975). The α value measures the relative efficiency of an earthquake of a certain magnitude in generating daughter events or aftershocks in a general sense.

Results

The ETAS parameters μ, K, c, p, and α of each earthquake sequence were determined using a maximum-likelihood method performed according to Ogata (1992), using the Davidon–Fletcher–Powell method (e.g., Fletcher and Powell, 1963). The confidence intervals for each of the estimated ETAS parameters were calculated using the inverse of the Hessian matrix of the log-likelihood function (see Coles [2007] for the theoretical background).

As mentioned before, while M_c is around 2.0 for the catalog under investigation, one should expect significantly larger M_c values at the beginning of aftershock sequences (Kagan, 2004; Peng *et al.*, 2006; Enescu *et al.*, 2007; Peng *et al.*, 2007; Enescu *et al.*, 2009). According to recent studies that focus on the beginning of aftershock sequences using high-resolution waveform data (e.g., Peng *et al.*, 2006; Enescu *et al.*, 2007; Peng *et al.*, 2007; Enescu *et al.*, 2009), a c value larger than several minutes is likely caused by missing small earthquakes. We therefore decided to select only sequences for which the c value estimated using the ETAS model is less than 20 min. We also tested other c value thresholds between 10 and 40 min and obtained similar results. In this way, when using sequences with a time length of 100 days, we end up with numbers of earthquake sequences $N_{seq} = 62$ and $N_{seq} = 37$ for $N_{bg} = 15$ and $N_{bg} = 5$, respectively. The number of separated sequences is decreasing when we use a shorter time length of 20 days: $N_{seq} = 45$ and $N_{seq} = 30$ for $N_{bg} = 15$ and $N_{bg} = 5$, respectively. When describing the results we refer to the first case ($N_{seq} = 62$, $N_{bg} = 15$) unless mentioned otherwise. We ran several ETAS parameter estimations starting from different initial conditions and found that the estimated parameter values are stable.

Figure 2a,b presents the result of stacking earthquake sequences as a function of the α value. We show the event stacks only for the time interval from −20 to 20 days relative to the mainshock because this time period contains most of the earthquakes and we would like to visualize this period better. The origin of the time axis corresponds to the mainshock occurrence time. The frequency of the events per day is normalized (i.e., divided by the maximum daily frequency) to make the results comparable. One can recognize the swarm-type characteristics for the stack in Figure 2a and the more typical foreshocks–mainshock–aftershocks sequence in Figure 2b. One can see the more pronounced foreshock activity in the case of small α (i.e., $\alpha < 1.4$) in Figure 2a, and the clear onset of aftershock activity for the case of large α (i.e., $\alpha \geq 1.4$) in Figure 2b. In contrast to the stacked data of Figure 2a, the results of Figure 2b show a clear increase of the number of earthquakes at small positive time compared to the background level in the day before the mainshock.

Figure 3 shows the decay of aftershock activity in the first 10 days from the mainshock for the stacked earthquake sequences characterized by the two different ranges of α values. The parameters of the Omori–Utsu law (equation 4) were estimated using a maximum-likelihood procedure (Ogata, 1983). We find a smaller p value ($p \sim 0.7$) for the swarm-type earthquake activity with $\alpha < 1.4$. This might be a consequence of a stronger impact of secondary aftershocks in the case of the swarm-type activity. In general, we notice that the p value for the stacked sequences is smaller than the values (around 1.0) usually obtained in the analysis of single sequences of earthquakes. Small p values have been often reported for superposed aftershock sequences (Utsu *et al.*, 1995) and may be caused by including sequences that mainly consist of background seismicity or are characterized by different c values. The estimation of the p values for the individual clusters using the ETAS model

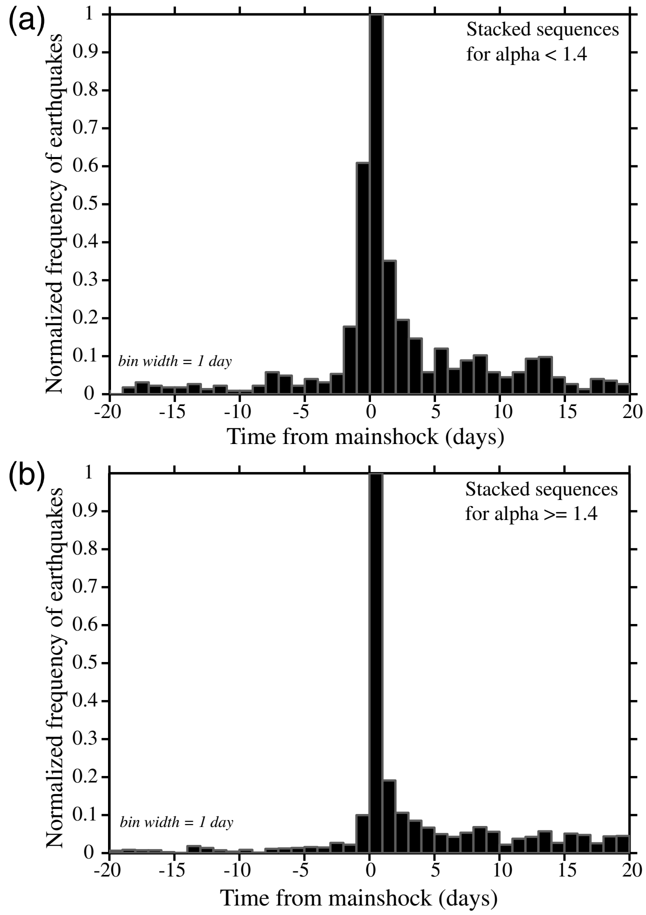

Figure 2. Normalized daily frequency of stacked earthquakes from −20 days before to 20 days after the mainshock. (a) Results for stacked sequences characterized by $\alpha < 1.4$. (b) Corresponding results for sequences characterized by $\alpha \geq 1.4$.

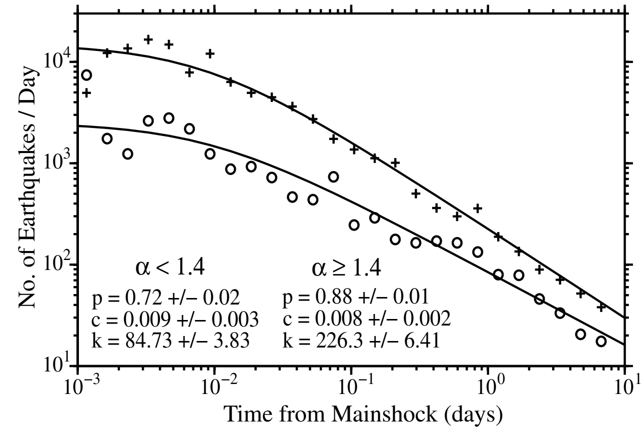

Figure 3. Decay of aftershocks activity versus time for stacked sequences with $\alpha < 1.4$ (circles) and $\alpha \geq 1.4$ (plus signs). The fit of the data by the Omori–Utsu law (equation 4) and the p, c, and K values for each case, determined as explained in the text, are also given.

shows in our case that most of the p values are between 0.9 and 1.4, in agreement with Utsu *et al.* (1995). The smallest p value obtained for individual sequences is 0.7 and the largest one is 1.8.

Figure 4 shows the spatial distribution of α values in the following three different ranges: small ($\alpha < 1.4$), intermediate ($1.4 \leq \alpha \leq 1.9$), and large ($\alpha > 1.9$) values. The geographic location of each symbol is the same as that of the mainshock epicenter of the corresponding earthquake sequence. The areas outlined by the dashed rectangles that are marked by A, B, and C in Figure 4 are characterized by relatively small values of α. Comparing with Figure 1, we note that the A, B, and C areas are also characterized by relatively large surface heat flow values. They geographically correspond to the Imperial-Mexicali Valley and Cerro Prieto geothermal field in Baja California (region A), the Coso geothermal area (region B), and the Long Valley caldera (region C). Thus, the map of α values confirms that the seismicity in the areas of high heat flow is mainly characterized by swarm-type behavior. We also stacked together the earthquake sequences with mainshocks that occurred inside areas A, B, and C and compare the results with the stack of sequences for which the mainshock occurred outside these boxes. The normalized frequency of events versus the relative time from the mainshock for the two cases is shown in Figure 5. It can be seen that the stacked sequences for the three regions, A, B, and C, of relatively high heat flow (Fig. 1) show the characteristic swarm-type pattern, similar with that in Figure 2a. On the other hand the stack of all the other sequences is similar to

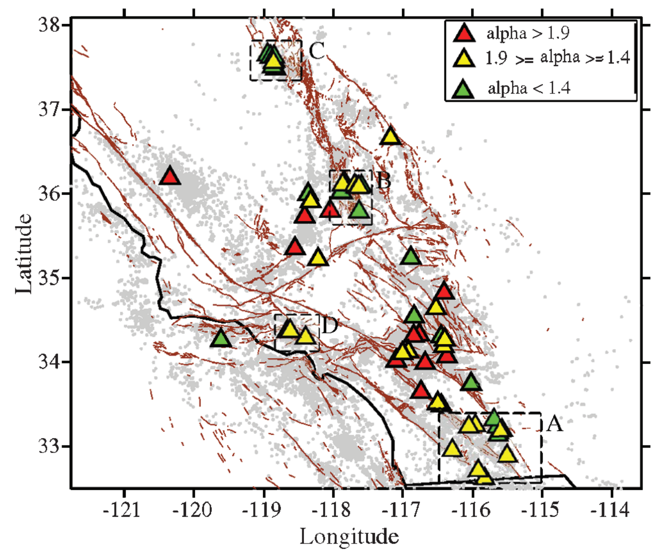

Figure 4. Spatial distribution of α values of the ETAS model (colored triangles as indicated in the legend). The areas A, B, and C outlined by dashed-line rectangles are characterized by relatively small α values and relatively large surface heat flows (see Fig. 1). These areas roughly correspond geographically to the Imperial-Mexicali Valley and Cerro Prieto geothermal field in Baja California (region A), the Coso geothermal area (region B), and the Long Valley caldera (region C). Rectangle D is characterized by average α values and relatively low heat flow and corresponds to the Ventura basin with a thick sedimentary cover.

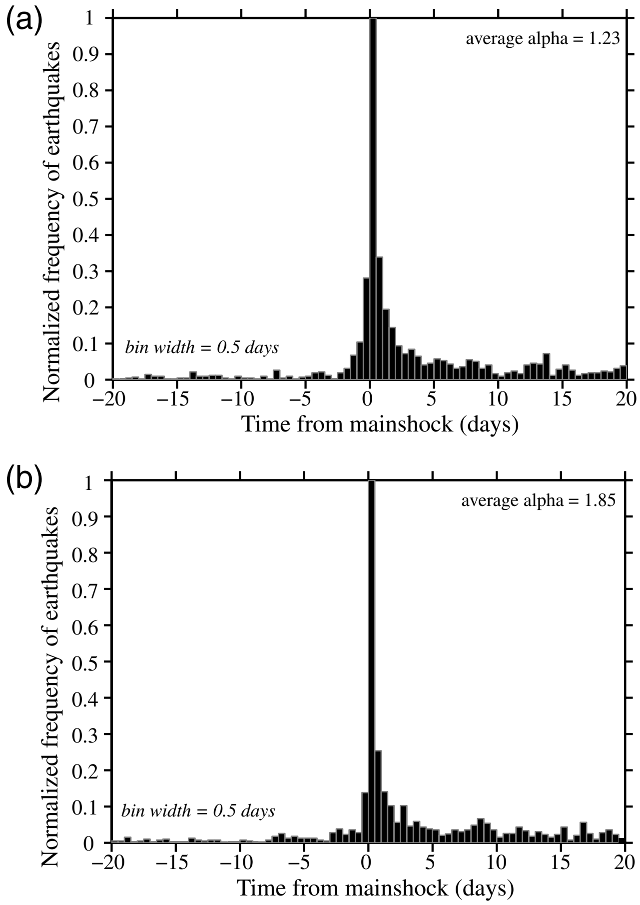

Figure 5. Normalized half-day frequency of stacked earthquakes from −20 to 20 days relative to the mainshock: (a) results for sequences with mainshocks that occurred in the areas A, B, or C; (b) results for sequences with mainshock that occurred outside these areas. The average α values for each case are also indicated.

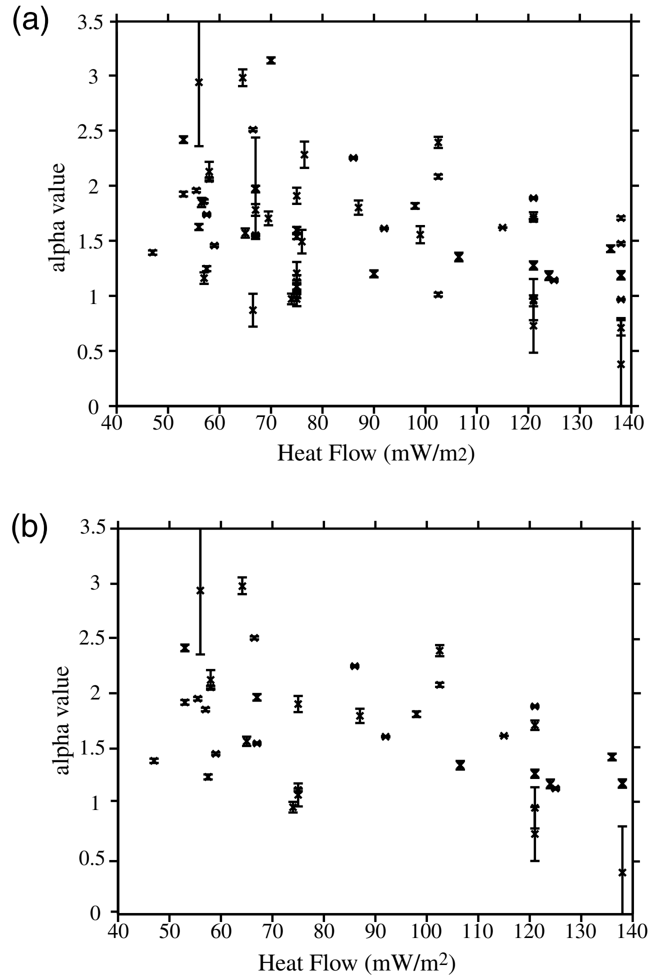

Figure 6. Mean heat flow versus α values for (a) $N_{bg} = 15$ and (b) $N_{bg} = 5$ in analysis using sequences from −100 to 100 days from their corresponding mainshock. The mean heat flows were calculated for a circular region with a radius of 60 km around the epicenters of the mainshocks of each earthquake sequence. The error bars represent confidence intervals that correspond to 1 standard deviation.

the foreshocks–mainshock–aftershocks pattern of Figure 2b. The average α values for the first and second case are 1.23 and 1.85, respectively. We also examined stacked earthquake sequences at each of the boxes, A, B, and C, individually and obtained the characteristic swarm-type pattern associated with a smaller α value. The occurrence patterns of earthquake sequences found here for low and high heat flow regions agree in general with those reported by Peng (2007).

It is of interest to have a quantitative assessment of how the regional heat flow and α values correlate. Toward this end we calculate the median heat flows in circles with a radius $R_{hf} = 60$ km centered at the locations of the mainshocks of each separated sequence. We used the median and not the average to suppress outliers. We first discuss the results obtained for sequences with a time length of 100 days. Figure 6a displays the obtained median heat flow values versus our derived α values in the same areas for the analysis with $N_{bg} = 15$ events. It is noticed that regions with large heat flow values have the smallest α values, in agreement with the observation made in Figures 4 and 5, although a few of the small α values have larger confidence limits. We can also see that for progressively smaller heat flows the α values have an increasing trend. However, the range of α values is relatively large, especially for small heat flow values. This generally agrees with the observation of Vidale and Shearer (2006) that swarm-type seismicity is not limited to volcanic or geothermal areas. Figure 6b presents a similar dependence between median heat flow and α values for the case $N_{bg} = 5$ events. The linear correlation coefficient between the α values and the median heat flow are −0.43 and −0.49 for the first (Fig. 6a) and second (Fig. 6b) case, respectively. If we split the α values into two groups that correspond to heat flows greater and smaller than 90 mW/m^2, the distributions are different at a 95% confidence level, as determined using the Kolmogorov–Smirnov statistical test.

Figure 7a,b presents the ETAS modeling results for earthquake sequences of shorter time length, spanning from

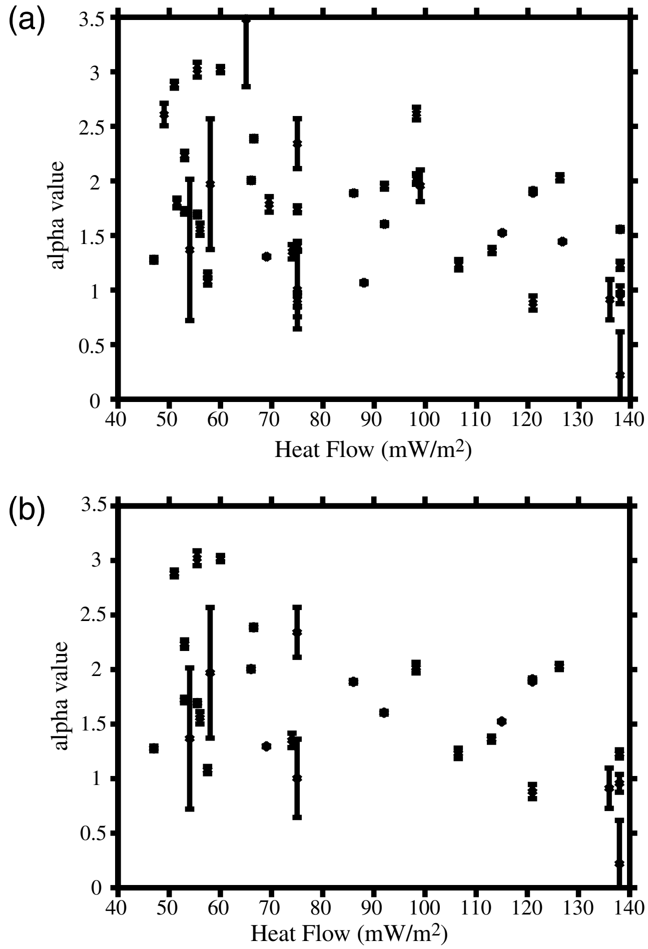

Figure 7. Same as for Figure 6 for sequences spanning between −20 to 20 days from the mainshock.

−20 days before to 20 days after the mainshock for $N_{bg} =$ 15 and $N_{bg} = 5$ events, respectively. While some differences exist, the variation of α versus heat flow is similar in general with that seen in Figure 6: there is a decrease of the relative aftershock productivity parameter for higher heat flow values, and there is a broader α distribution at lower heat flows. This shows that the correlation discussed previously is robust and does not change significantly if the time length of sequences is shortened. The linear correlation coefficients are −0.42 and −0.47 for the first case (Fig. 7a) and second case (Fig. 7b), respectively. If we separate the sequences into two groups with heat flows greater or less than 90 $\mathrm{mW/m^2}$, the corresponding α value distributions differ at the 95% confidence level.

Discussion

The results presented in the first part of the Results section indicate that regions of relatively high heat flow are characterized by a swarm-type temporal distribution of seismicity and a relatively small α, while areas with lower heat flow display a foreshock–mainshock–aftershock pattern and higher values of the relative productivity parameter. The quantitative correlation of α with the median heat flow values is moderate (with a correlation coefficient of about 0.4), but a separation of α values into two groups of low and high heat flows reveals that the two distributions are statistically different at a high confidence level.

The results shown in the previous section were obtained using fixed constant values for some parameters (e.g., M_{c}, N_{bg}, and R_{hf}). Without claiming that we explored all possible parameters, the presented results were carefully checked for stability. For example, Figures 6 and 7 lead to a similar conclusion. We also analyzed the data using threshold magnitudes from 2.1 to 2.4, and, while the number of separated sequences is decreasing, similar conclusions can be drawn. For example, using a threshold magnitude of 2.3, sequences spanning from −20 to +20 days relative to the mainshock and $N_{bg} = 15$, we obtained a linear correlation coefficient of 0.39 and α-value distributions that are different at the 90% confidence level. If the threshold magnitude is further increased, the number of separated sequences becomes small, with only 11 sequences for a threshold magnitude of 3.0. In such a case, the correlation analysis applied for lower threshold magnitudes becomes inconclusive. However, the stacking of sequences in low and high heat flow regions still produces significantly different results. This is illustrated by stacking the earthquake sequences in regions A, B, and C (Fig. 8a) and in the rest of the study area (Fig. 8b) using a threshold magnitude of 2.6. The foreshock–aftershock pattern is the same as discussed earlier in the context of Figure 5. The average alpha values, with errors of less than 0.3, are 1.55 and 2.34, for the areas with high and low heat flows, respectively. In the case of R_{hf}, we also checked a range of values and found that the overall features observed in Figures 6 and 7 do not change significantly for R_{hf} between about 50 and 70 km. We speculate that such a range of values may reflect the regional heat flow conditions that influence the temporal and spatial behavior of seismicity. At more local scales additional factors like the presence of fluids (e.g., Hainzl and Ogata, 2005; Vidale and Shearer, 2006; Mori *et al.*, 2008) and overall category of rock type (e.g., crystalline versus sediments) may play an important role in governing aspects of the seismicity. The correlation coefficient between the α values and the median heat flow is for all analyzed cases between −0.35 and −0.52, while the α value distributions for low and high heat flow areas are different at confidence levels higher than 85%.

We also tested our results using a different approach, independent of R_{hf}, for correlating the α values with the heat flow. Using a linear interpolation method we obtained heat flow values at the epicenter location of the mainshock of each earthquake sequence. Figure 9 shows results obtained for sequences separated using a time length of 100 days and $N_{\mathrm{bg}} = 15$ events (same as for Fig. 6a). The range of the interpolated heat flow values in Figure 9 is seen to be larger than the spread of the median heat flow values (Fig. 6a). Moreover, the α values appear generally clustered into two groups with

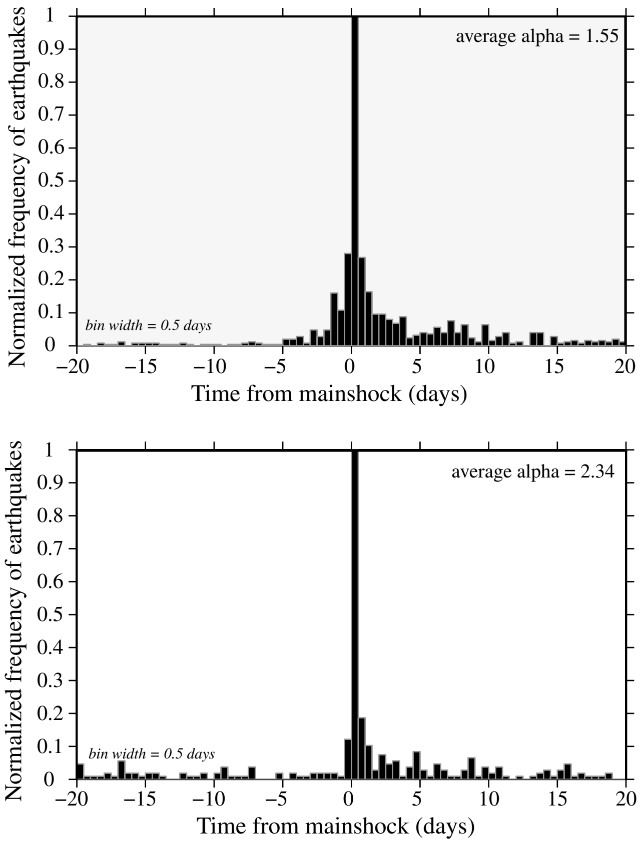

Figure 8. Same as for Figure 5 for a threshold magnitude of 2.6. The average α values for each case are also indicated.

heat flow values between 30 and 100 mW/m^2 and 130 and 200 mW/m^2, respectively. We interpret these differences as resulting mainly from outliers in the heat flow data; indeed if one uses the mean instead of the median to calculate the heat flow values in Figure 6a, a similar spread of the heat flow results and clustering of α values as in Figure 9 can be observed. However, the Kolmogorov–Smirnov test applied

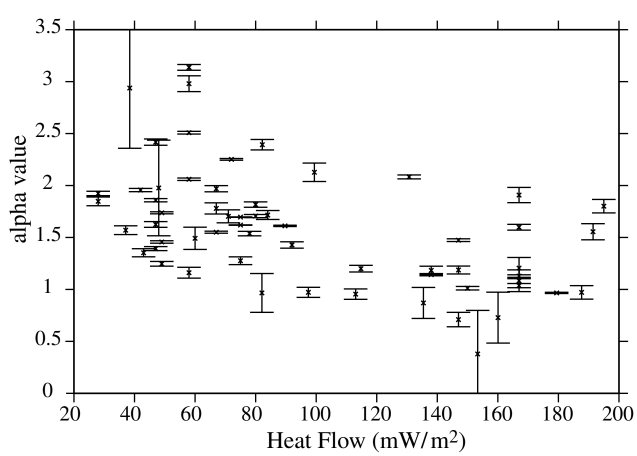

Figure 9. Same as for Figure 6a using interpolated heat flow values at the epicenter location of the mainshock of each separated sequence.

to the data in Figure 9 reveals that the two groups of α values that correspond to relatively low and high heat flows, respectively, are different at a 95% confidence level. The correlation coefficient between the heat flow and α values is -0.36.

As discussed by Helmstetter *et al.* (2005), α values estimated by fitting the ETAS model to the data are often significantly smaller than those determined from the stacking of aftershock sequences. Hainzl *et al.* (2008) have shown that the bias results mainly because of the anisotropy problem (see the Analysis Method section), which is avoided if one uses a space-independent ETAS approach like the one used in this study. Please note that the alternative approach to estimate the α values by stacking sequences with mainshocks in different magnitude bins (e.g., Felzer *et al.*, 2004) is not applicable in our case. Our goal is to reveal spatial correlations, and thus, the number of sequences in subvolumes with relatively large and low heat flows is not large enough to apply this procedure. We therefore need to estimate the parameters for individual sequences, with the drawback that we are limited to the analysis of more active ones.

Our α estimates have uncertainties stemming from the assumptions we make and the limited data sets. The uncertainties that we determine and plot in Figures 6, 7, and 9 may reflect only part of these errors. However, the statistical analysis we performed and the examination of each separated sequence confirmed that the obtained correlations are robust and reflect physical properties of the crust.

It is worth mentioning that the use of the heat flow data also has some shortcomings. From Figure 1 it can be seen that some areas of dense seismicity have only several heat flow measurements, while other areas with scarce seismicity are better covered with heat flow measurements. Moreover, we do not have information about the uncertainties of these data. However, the use of the median of heat flow values measured in a relatively large circular region (of radius R_{hf}) alleviates to some extent these problems.

The viscoelastic damage rheology model of Ben-Zion and Lyakhovsky (2006) predicts that the aftershock productivity is proportional to the effective viscosity in a region. Thus, the productivity of aftershocks should decrease for lithological and ambient conditions that reduce the viscosity. These include increasing temperature, high fluid content, and existence of thick sediments that have relatively low viscosity. Our results show that high heat flow regions are characterized in general by low α values, which is consistent with the predictions of the damage rheology model. The area marked by D in Figure 5 corresponds roughly to the Ventura basin, known for its thick sedimentary cover. The α values obtained for this region are average while the heat flow values (Fig. 1) are on the low side. This is in general agreement with the damage model prediction, although the number of sequences is too small to draw strong conclusions. Yang and Ben-Zion (2009) provide additional evidence for correlations between aftershocks productivity, heat flow, and thickness of sedimentary cover using a different approach based on estimation of the Omori–Utsu law parameters for several different regions in southern California. We have also obtained absolute productivity estimates by integrating the Omori–Utsu formula between 0 and the time length of the aftershocks in each sequence, using as input the K, α, p, and c values obtained from the fit of the ETAS model, as well as the mainshock magnitude M and the threshold magnitude M_c. However, these estimations have rather high uncertainties because they are obtained using input parameters that have their own estimation errors. Therefore, our analysis with absolute values does not show a clear correlation with the heat flow data.

We also looked in this study for possible correlations between the α values and the depth of the mainshock of each sequence but did not find any clear relation. We noticed a broader range of α values for sequences with shallow mainshocks, while deeper mainshocks were associated with average α values (around 1.5). It may be of interest to take into account the faulting style of each of the mainshocks (Peng, 2007) when analyzing the previous correlations, but the statistics will become less convincing due to the small number of available sequences.

We also investigated possible correlations between other seismicity parameters and the surface heat flow. Mogi (1963), for example, analyzed Japanese earthquake data and found faster aftershock decays (i.e., higher p values) in regions of higher crustal temperature. In our case, five of the sequences that occurred in region A were characterized by relatively large p values, ranging from 1.4 to 1.8. However, a systematic analysis shows a relatively weak correlation with the median heat flows (correlation coefficient of 0.2).

Conclusions

We applied a systematic procedure to search for sequences of earthquakes that are well separated in time and space from other seismicity and used the ETAS model to determine the statistical characteristics of these sequences. Our results can be summarized as follows:

1. The estimated α parameter of the ETAS model, which measures the relative efficiency of an earthquake of a certain magnitude to produce aftershocks, could be successfully used to distinguish between swarm-type and more typical earthquake sequences. The two different categories are characterized by relatively small and relatively large α values, respectively.
2. The swarm-type sequences have significantly more foreshocks than the other more typical sequences. The stacked sequences of the latter show a clear increase in the number of earthquakes in the day preceding the mainshock.
3. The areas of high heat flow are characterized by relatively small α values, and there is a positive correlation between increasing crustal heat flow and decreasing α values.
4. The findings of this study are generally consistent with predictions of the damage rheology model of Ben-Zion and Lyakhovsky (2006) that relates regional conditions to values of rheological parameters and aftershock productivity. However, the scatter of α values for low or high heat flow values is relatively large. We assume that this is related to other factors, like the presence of fluids, which can have additional strong effects on the temporal and spatial characteristics of seismicity.

Data and Resources

The heat flow data is taken from the USGS online heat flow database: http://earthquake.usgs.gov/heatflow/index.html (last accessed last January 2009).

Acknowledgments

We thank Yoshi Ogata for useful comments on an earlier version of this work. Zhigang Peng kindly provided the results of his analysis and useful suggestions. We thank Danijel Schorlemmer and Michael Lewis for useful discussions on the magnitude of completeness issues and providing their M_c results for Southern California. B. E. and S. H. acknowledge financial support from the European Union project SAFER (Contract Number 036935). Y. B. Z. acknowledges support from the Southern California Earthquake Center (based on National Science Foundation Cooperative Agreement EAR-0106924 and U.S. Geological Survey Cooperative Agreement 02HQAG0008). The manuscript benefited from useful comments by Karen Felzer, an anonymous reviewer, and Associate Editor Stefan Wiemer.

References

Ben-Zion, Y. (2003). Key formulas in earthquake seismology, *International Handbook of Earthquake and Engineering Seismology*, Part B, Academic Press, London, 1857–1875.

Ben-Zion, Y., and V. Lyakhovsky (2006). Analysis of aftershocks in a lithospheric model with seismogenic zone governed by damage rheology, *Geophys. J. Int.* **165,** 197–210.

Ben-Zion, Y., and L. Zhu (2002). Potency-magnitude scaling relations for southern California earthquakes with $1.0 < M_L < 7.0$, *Geophys. J. Int.* **148,** F1–F5.

Christophersen, A., and E. G. C. Smith (2008). Foreshock rates from aftershock abundance, *Bull. Seismol. Soc. Am.* **98,** 2133–2148.

Coles, S. (2007). *An Introduction to Statistical Modeling of Extreme Values*, Springer-Verlag, London, 31–33.

Enescu, B., and K. Ito (2002). Spatial analysis of the frequency-magnitude distribution and decay rate of aftershock activity of the 2000 Western Tottori earthquake, *Earth Planets Space* **54,** 847–859.

Enescu, B., J. Mori, and M. Miyazawa (2007). Quantifying early aftershock activity of the 2004 mid-Niigata Prefecture earthquake (M_w 6.6), *J. Geophys. Res.* **112,** B04310, doi 10.1029/2006JB004629.

Enescu, B., J. Mori, M. Miyazawa, and Y. Kano (2009). Omori–Utsu law c-values associated with recent moderate earthquakes in Japan, *Bull. Seismol. Soc. Am.* **99,** no. 2A, 884–891, doi 10.1785/0120080211.

Felzer, K. R., and E. E. Brodsky (2006). Decay of aftershock density with distance indicates triggering by dynamic stress, *Nature* **441,** 735–738.

Felzer, K. R., R. E. Abercrombie, and G. Ekström (2004). A common origin for aftershocks, foreshocks, and multiplets, *Bull. Seismol. Soc. Am.* **94,** 88–98.

Fletcher, R., and M. J. D. Powell (1963). A rapidly convergent descent method for minimization, *Comput. J.* **6,** 163–168.

Gutenberg, R., and C. F. Richter (1944). Frequency of earthquakes in California, *Bull. Seismol. Soc. Am.* **34,** 185–188.

Hainzl, S. (2003). Self-organization of earthquake swarms, *J. Geodyn.* **35,** 157–172.

Hainzl, S. (2004). Seismicity patterns of earthquake swarms due to fluid intrusion and stress triggering, *Geophys. J. Int.* **159,** 1090–1096, doi 10.1111/j.1365-246X.2004.02463.x.

Hainzl, S., and Y. Ogata (2005). Detecting fluid signals in seismicity through statistical earthquake modeling, *J. Geophys. Res.* **110,** B05S07, doi 10.1029/2004JB003247.

Hainzl, S., A. Christophersen, and B. Enescu (2008). Impact of earthquake rupture extensions on parameter estimations of point-process models, *Bull. Seismol. Soc. Am.* **98,** 2066–2072, doi 10.1785/0120070256.

Helmstetter, A., Y. Kagan, and D. Jackson (2005). Importance of small earthquakes for stress transfers and earthquake triggering, *J. Geophys. Res.* **110,** B05S08, doi 10.1029/2004JB003286.

Kagan, Y. Y. (2004). Short-term properties of earthquake catalogs and models of earthquake source, *Bull. Seismol. Soc. Am.* **94,** 1207–1228.

Kanamori, H., and D. L. Anderson (1975). Theoretical basis of some empirical relations in seismology, *Bull. Seismol. Soc. Am.* **65,** 1073–1095.

Lin, G., P. Shearer, and E. Hauksson (2007). Applying a three-dimensional velocity model, waveform cross-correlation, and cluster analysis to locate southern California seismicity from 1981 to 2005, *J. Geophys. Res.* **112,** B12309, doi 10.1029/2007JB004986.

Lohman, R. B., and J. J. McGuire (2007). Earthquake swarms driven by aseismic creep in the Salton trough, California, *J. Geophys. Res.* **112,** B04405, doi 10.1029/2006JB004596.

Mogi, K. (1963). Some discussions on aftershocks, foreshocks, and earthquake swarms: The fracture of a semi-infinite body caused by an inner stress origin and its relation to the earthquake phenomenon, *Bull. Earthq. Res. Inst., Univ. Tokyo* **41,** 615–658.

Mori, J., Y. Kano, and B. Enescu (2008). Comparison of early aftershock sequences for the 2004 Mid-Niigata and 2007 Noto Hanto earthquakes in central Japan, *Earth Planets Space* **60,** 151–154.

Nur, A. (1974). Matsushiro, Japan earthquake swarm: Confirmation of the dilatancy-fluid diffusion model, *Geology* **2,** 217–221.

Ogata, Y. (1983). Estimation of the parameters in the modified Omori formula for aftershock frequencies by the maximum likelihood procedure, *J. Phys. Earth* **31,** 115–124.

Ogata, Y. (1985). Statistical models for earthquake occurrences and residual analysis for point processes, *Res. Memo (Technical Report)*, **288,** Inst. Statist. Math., Tokyo.

Ogata, Y. (1987). Long term dependence of earthquake occurrences and statistical models for standard seismic activity, *Suri Zisin Gaku*, Mathematical Seismology II, M. Saito (Editor), Cooperative Research Report 3, Inst. Statist. Math., Tokyo, 115–124 (in Japanese).

Ogata, Y. (1988). Statistical models for earthquake occurrences and residual analysis for point-processes, *J. Am. Statist. Assoc.* **83,** 9–27.

Ogata, Y. (1992). Detection of precursory relative quiescence before great earthquakes through a statistical model, *J. Geophys. Res.* **97,** 19,845–19,871.

Peng, Z. (2007). Occurrence patterns of foreshocks and aftershocks in southern California, *Seism. Res. Lett.* **78,** 269.

Peng, Z., J. E. Vidale, and H. Houston (2006). Anomalous early aftershock decay rate of the 2004 M_w 6.0 Parkfield, California, earthquake, *Geophys. Res. Lett.* **33,** L17307, doi 10.1029/2006GL022626.

Peng, Z., J. E. Vidale, M. Ishii, and A. Helmstetter (2007). Seismicity rate immediately before and after mainshock rupture from high-frequency waveforms in Japan, *J. Geophys. Res.* **112,** B03306, doi 10.1029/2006JB004386.

Reasenberg, P. (1985). Second-order moment of central California seismicity, 1969–1982, *J. Geophys. Res.* **90,** 5478–5495.

Richter, C. F. (1958). *Elementary Seismology*, Freeman, San Francisco, 768 pp.

Schorlemmer, D., and J. Woessner (2008). Probability of detecting an earthquake, *Bull. Seismol. Soc. Am.* **98,** 2103–2117, doi 10.1785/0120070105.

Sykes, L. R. (1970). Earthquake swarms and sea-floor spreading, *J. Geophys. Res.* **75,** 6598–6611.

Utsu, T., and A. Seki (1955). Relation between the area of aftershock region and the energy of the main shock, *J. Seismol. Soc. Jpn.* **7,** 233–240 (in Japanese).

Utsu, T., Y. Ogata, and R. S. Matsu'ura (1995). The centenary of the Omori formula for a decay law of aftershock activity, *J. Phys. Earth* **43,** 1–33.

Vidale, J. E., and P. M. Shearer (2006). A survey of 71 earthquake bursts across southern California: Exploring the role of pore fluid pressure fluctuations and aseismic slip as drivers, *J. Geophys. Res.* **111,** B05312, doi 10.1029/2005JB004034.

Wiemer, S., and M. Wyss (2000). Minimum magnitude of complete reporting in earthquake catalogs: Examples from Alaska, the western United States, and Japan, *Bull. Seismol. Soc. Am.* **90,** 859–869.

Woessner, J., and S. Wiemer (2005). Assessing the quality of earthquake catalogs: Estimating the magnitude of completeness and its uncertainties, *Bull. Seismol. Soc. Am.* **95,** 684–698, doi 10.1785/0120040007.

Working Group on California Earthquake Probabilities (2003). Earthquake probabilities in the San Francisco Bay region: 2002–2031, *U.S. Geol. Surv. Open-File Rept. 03-214*.

Yang, W., and Y. Ben-Zion (2009). Observational analysis of correlations between aftershocks productivities and regional conditions in the context of a damage rheology model, *Geophys. J. Int.* **177,** 481–490.

GFZ German Research Centre for Geosciences
Telegrafenberg, Potsdam
14473, Germany
benescu@bosai.go.jp
(B.E., S.H.)

Department of Earth Sciences
University of Southern California
Los Angeles, California 90089-0740
(Y.B.)

Manuscript received 23 April 2008